Computational analysis of a radiofrequency knee coil for low-field MRI using FDTD

Valentina Hartwig,[1,3] Stefano Tassano,[2] Alessio Mattii,[3] Nicola Vanello,[3] Vincenzo Positano,[4] Maria Filomena Santarelli,[1] Luigi Landini,[3,4] Giulio Giovannetti[1]

[1]Institute of Clinical Physiology, CNR, Pisa, Italy

[2]Paramed srl, Genova, Italy

[3]Department of Information Engineering, University of Pisa, Italy

[4] Fondazione G. Monasterio CNR-Regione Toscana, Pisa, Italy

Corresponding author:

Eng. VALENTINA HARTWIG, PhD

Institute of Clinical Physiology (IFC) - Italian National Research Council (CNR)

Via G. Moruzzi 1

56124 San Cataldo (Pisa) - Italy

Tel: +39 050 3152827

Fax: +39 050 3152166

E-mail: valeh@ifc.cnr.it

Abstract

Magnetic Resonance Imaging (MRI) is essential for the diagnosis and treatment of musculoskeletal conditions. Low-field (< 0.5T) imaging is a cost-effective alternative to more expensive high-field strength imaging due to the inexpensive setting, greater patient comfort and better safety profile. On the other hand, if compared with high-field body scanners, the low-field scanners produce poor-quality images with lower signal-to-noise ratio (SNR). Especially in low-field MR, receiver coil performance plays a significant role in image quality. Coil performance is generally evaluated using classical electromagnetic theory, but when the coil is loaded with a sample, an analytical solution is extremely difficult to derive, so that a trial-and-error approach is often followed. Numerical methods have been proposed in literature as good alternatives to predict MRI coil performance. In this study the performance of a knee coil for low-field (0.5 T) MR scanners is analyzed using workbench tests and numerical simulation with a software program based on the finite difference time domain method (FDTD). Parameter performances measured using the classical workbench test are compared with those obtained using numerical simulations. Finally, the knee coil performance is validated with images acquired in a commercial low-field MR system.

Keywords (4) FDTD method, low-field MRI, numerical simulation, RF coil

1. INTRODUCTION

Magnetic Resonance Imaging (MRI) is essential for the diagnosis and treatment of musculoskeletal conditions. Scanners with low (< 0.5T) and medium fields (0.5-1.5T) can be very useful for imaging the upper and lower extremities. Low-field MR extremity imaging offers further advantages such as a more convenient and cheaper setting, greater patient comfort and high diagnostic power. Moreover, MRI at low-field strengths has a better safety profile (1-4). On the other hand, if compared with high-field body scanners, low-field scanners produce poor-quality images with lower signal-to-noise ratio (SNR) that generally increases with field strength. However, a worse image quality does not necessarily translate into lower diagnostic accuracy in many situations (5-6). Therefore, in similar cases low-field imaging is a cost-effective alternative to the more expensive high- field strength imaging (7).

Radiofrequency (RF) coils performance plays a significant role in image quality, especially in low-field scanners. In order to obtain high quality information, RF coils should be able to support large field-of-view (FOV) with high RF magnetic field homogeneity in transmission as well as to achieve high SNR in reception (8). SNR is a function of the electromagnetic field generated by the coil which interacts with the sample to be imaged. Moreover, the use of coils that fit around parts of the body to be imaged is recommended for obtaining detailed images (9).

Electromagnetic theory can lead to analytical expression to estimate performance parameters for simple cases of surface coils, but is very difficult to use for solving more complex geometries. Moreover, when the coil is loaded with a sample, the distribution of SNR is affected by the electromagnetic properties of the sample, and in this case an analytical solution is extremely difficult to derive. For this reason, most MRI coil development has been done using a trial-and-error approach. Numerical methods have been proposed in literature as good alternatives to electromagnetic theory and the trial-and-error method to simulate MRI coils and predict their performances (10-16).

The main goal of this work was to show the possibility of using finite difference time domain method (FDTD) (10-14) for an accurate analysis of dedicated RF coils in terms of quality parameters. To make the procedure tractable, in this study we will focus on the analysis of the performance of a commercial two-channel knee coil for low-field (0.5 T) MR scanners, using workbench tests and numerical simulations with a software based on FDTD method. Sample resistance coil, sensitivity distribution and magnetic field homogeneity are evaluated. Parameter performances measured using workbench tests are compared with those obtained using numerical simulations. Despite this work focuses on a commercially available coil, the

methodology presented here could be also followed for the construction of a novel coil effectively before manufacturing.

2. THEORY

2.1 Coil perfomances

From the resonant circuit theory, it is established that the quality factor for an unloaded coil is:

$$Q_{unloaded} = \frac{\omega L_{coil}}{R_{coil}} \tag{1}$$

where ω is the angular frequency and L_{coil} and R_{coil} are the inductance and the resistance of the coil, respectively. From the knowledge of unloaded coil quality factor, by using Eq. 1 it is possible to obtain the R_{coil}. Similarly, when the coil is loaded, the quality factor can be calculated as:

$$Q_{loaded} = \frac{\omega L_{coil}}{R_{sample} + R_{coil}} \tag{2}$$

where R_{sample} is the sample-induced resistance.

2.2 Sample-induced resistance calculation by FDTD simulation

The sample induced resistance can be also estimated using an electromagnetic method (17-19) based on the classical resonant circuits theory. Remembering that the energy stored by a capacitor is proportional to the square of the voltage across its layers, the system quality factor Q can be expressed as (17):

$$Q = 2\pi \frac{V_i^2}{V_i^2 - V_{i+1}^2} \tag{3}$$

where V_i and V_{i+1} are, respectively, the voltage at i_{th} cycle and at $(i+1)_{th}$ cycle.

When the coil is made of a perfect electric conductor, the energy is dissipated only within the sample, so the sample-induced resistance R_{sample} can be calculated as:

$$R_{sample} = \frac{2\pi f_0 L_{coil}}{Q} \tag{4}$$

where f_0 is the Larmor frequency and L is the coil inductance value.

2.3 Coil sensitivity and magnetic field homogeneity

Coil sensitivity is defined as the magnetic field (B_1) induced by the RF coil at a given point per unit of supplied power (20). To estimate the coil sensitivity map is possible to calculate the magnetic field distribution.

Another important parameter in RF coil design is B_1 field homogeneity, since non-uniformity of the B_1 leads to unwanted variation in MR images (21). To evaluate the B_1 field homogeneity is possible to calculate the maximum relative deviation RD of the B_1 field for the solenoid channel as follows (22):

$$RD = \left| \frac{(B_1 - B_1 mean)}{B_1 mean} \right|_{\max} \cdot 100\% \tag{5}$$

where B_1mean is the calculated mean B_1 field in the homogeneous cylindrical phantom region.

3. MATERIALS AND METHODS

3.1 Workbench test of knee coil

A dedicated knee coil to be used with a commercial low-field MR scanner (MROpen, Paramed Medical Systems srl, Italy) was considered as a generic example to analyze in this work. The coil has two separate channels: a solenoid channel and a superficial one (Fig. 1). Both channels were realized with copper strips (70 μm thickness, 10 mm width). The solenoid channel consists of four identical loops 10 mm apart, while the superficial one consists of three loops 4 mm apart. The maximum size of the complete knee coil is 182x184x146 mm.

The decoupling of the two channels is automatically obtained given the topology of the two channels and their relative position (geometrical decoupling). Measured decoupling is -35 dB. Both channels are connected to the MR scanner by means a matching network (Fig. 2) followed by a differential pre-amplifier with a noise figure < 0.8.

The *Q* measurement was performed according to the definition (Eq. 1 and 2) with the coil in unloaded condition and then in two different loaded conditions. In the first condition the load was a cylindrical phantom filled with a saline solution (5mM $NiCl_2$ + 55mM NaCl) whose dielectric properties meet the American Society for Testing and Material (ASTM) criteria for

MR phantom developing (23) (electric conductivity=0.6 S/m, relative permittivity= 80) (24): the phantom had a diameter of 115 mm, a density of 1059 kg/m^3 and was 220 mm long, and was placed at the center of the coil volume solenoid channel. In the second loaded condition the load was the knee of an adult male volunteer (age 33, height 188 cm, weight 95 Kg). The inductance L_{coil} and the quality factor Q of each knee coil channel was evaluated by workbench test using a network analyzer (N9320B, Agilent) and a dual loop probe (20). This kind of measurement doesn't require any impedance matching between coil and network analyzer. Finally, measuring the loaded coil quality factor and using Eq. 2 the sample-induced resistance was obtained for each channel.

3.2 FDTD simulations

All numerical simulations were performed using commercially available software XFdtd (Remcom, State College, PA, USA). The knee coil CAD model was imported in the geometry tool and the Perfect Electric Conductor (PEC) was assigned as material.

Each unloaded channel was tuned to the operating frequency of 21.3 MHz (which is the corresponding Larmor frequency for a static magnetic field of 0.5 T) using four capacitors of 68 pF for the solenoid channel (Fig. 1 c) and four capacitors of 150 pF plus two of 180 pF for the superficial one (Fig. 1 d). The number of capacitors and their value and position have been chosen to match the commercial coil design. The inductance L for each channel was also calculated using the operating frequency and the total capacitance values.

The knee coil is designed for receive-only use, but its receive characteristics can be determined by simulating it in transmit mode according to the principle of reciprocity (25). Two different loads were used for the estimation of coil performance: a homogeneous cylindrical phantom and a human voxel model. The cylindrical phantom model had the same geometrical and electrical characteristics of the phantom used for the workbench tests and was placed at the center of the coil volume solenoid channel, which is also the origin of our reference system (Fig. 3 a).

The human voxel model employed is a volumetric model of an adult man (age 39, height 180 cm, weight 90 Kg), based on the scans from the National Library of Medicine's Visible Human male project. The model consisted of 39 tissues types to which we assigned appropriate electric conductivity, relative permittivity and mass density (26). The human model was placed in order to center the knee in the origin of our reference system (Fig. 3).

An automatic non-uniform mesh was chosen with a cell size of 1.3x1.3x1.3 mm in the knee volume. A time step of 1.75ps was chosen and the simulation was run for 200,000 steps with

an automatic detection of the convergence. In order to truncate outward waves and therefore simulate infinite radiation boundary conditions of the computational domain, we used perfect matched layer (PML) (22).

To calculate the sample induced resistance each channel was fed with a Gaussian pulse of amplitude equal to 1 V (17). The Gaussian pulse causes a perturbation which produces a damped voltage oscillation on the capacitors, required to estimate the sample resistance by Eq. 3.

Following, in a simulation with a sinusoidal input at the desired frequency of 21.3 MHz (@ 1A amplitude) (26), the magnetic field B_1 distribution across the center of each coil channel loaded with the human knee model has been calculated for axial, sagittal and coronal planes. For each channel loaded with homogeneous cylindrical phantom the profile of the B_1 field is also reported versus the y-axis.

The relative deviation RD was calculated using B_1 field distribution in the homogeneous cylindrical phantom (@ 70x70 mm^2 central ROI) according to Eq. 5.

3.3 Imaging

All images in this work were acquired with the 0.5 T scanner MROpen (Paramed Medical Systems srl, Genova, Italy).

To acquire the images of the homogenous cylindrical phantom for each coil channel a SPIN ECHO sequence was used (TE = 24 ms, TR = 500 ms, FOV 30x30 cm^2, matrix 256x256, Slice thickness 5 mm, Echo Number 1, Spacing Between Slices 10 mm, Flip Angle 90°, Number of Averages 1).

From these images the B_1 field profile for each channel was extracted using the following equation (27):

$$S = B_1 \cdot C \tag{6}$$

where S is the MR image (the intensity value of image pixels) and C is the acquired signal from the cylindrical phantom. Since the phantom is highly homogeneous, C can be considered as a constant so the magnetic field profile can be directly estimated from the pixel values in the images (27).

For calculation of field homogeneity in the solenoid channel the maximum relative deviation RD was calculated using Eq. 5 and the pixel values in a 70x70 mm^2 central ROI of the image.

4. RESULTS

4.1 Workbench test results

The measured inductance values L_{coil} were 3.761 μH and 2.433 μH for the solenoid channel and the superficial channel respectively.

Table 1 shows the measured knee coil performance (resonance frequency f_0, bandwith @-3dB B, quality factor Q) and the calculated sample-induced resistance R_{sample} and coil resistance R_{coil}. All parameters are shown for each knee coil channel (SOL = solenoid channel, SUP = superficial channel) in three different load conditions: unloaded, loaded with cylindrical phantom and loaded with a human knee (of a male volunteer).

4.2 FDTD Simulation results

L_{coil} calculated using simulation were 3.2842 μH for the solenoid channel and 2.109 μH for the superficial channel.

Table 1 shows the sample-induced resistance R_s. The tuning frequency values for each case are also reported.

To compare the sample-induced resistance estimated using XFdtd simulations with the one measured using the workbench test, we calculated the relative error, reported in Table 1. Before calculating the error, the sample-induced resistance Rs were adjusted to the Larmor frequency of 21.3 MHz considering the frequency dependence of the sample noise contribution (28).

Figure 4 shows the B_1 field distribution across the center of each coil channel loaded with the human knee model for axial, sagittal and coronal planes. The dB values are relative to the B_1 in the center of the coil.

Figure 5 (a, b) shows the profile of the B_1 field for the two channels in three different conditions: unloaded, loaded with the homogeneous cylindrical phantom and loaded with the human model. Note that the three profiles are very similar: this is expected given the low field value (29). Red points in the graphs indicate the phantom extension along the y-axis.

Moreover, as expected, the B_1 profile for the solenoid channel is symmetric and uniform since the solenoid is a kind of “volume coil”, while the magnetic field intensity for the superficial channel decreases with increasing distance from the coil (which is placed at y = 100 mm).

For the solenoid channel the maximum relative deviation RD of the B_1 field, calculated according the Eq. 5 was equal to 12%.

4.3 Imaging Results

Figure 5 (c, d) shows the plot of the B_1 field as a function of the y-axis for each channel coil loaded with homogeneous cylindrical phantom. The dashed line is relative to the plot obtained from the acquired images while the solid line is relative to the plot obtained from the simulation.

The maximum relative deviation RD of the B_1 field for the solenoid channel, calculated using the acquired image for the homogeneous cylindrical phantom, was equal to 13.91%.

5. DISCUSSION AND CONCLUSION

The main goal of this work was to show the possibility of using FDTD algorithm for an accurate analysis of dedicated RF coils in terms of quality parameters.

To make the procedure tractable a commercial dedicated knee coil for low-field MR imaging was chosen: we compared workbench measure of standard quality parameters of this coil with performance analysis carried out using numerical simulations based on the FDTD method.

For the sample-induced resistance calculation, the coil model has to be first tuned at Larmor frequency. Successively, after the application of the Gaussian pulse which perturbs the resonant circuit, it is necessary wait for the complete vanish of the transient effects.

Since the sample-induced resistance method has to be applied after the coil resonant frequencies calculation, we think that it can be used for multimodal resonant spectrum coil (such as birdcage coil) by choosing the parameters of the Gaussian pulse in dependence on the investigated resonant mode.

According to our results the estimation of R_{sample} for homogeneous cylindrical phantom is very accurate, since the relative error between the simulation results and workbench test results is lower than 5 %, for both channels. The relative error for the superficial channel loaded with the human model is greater: this is probably due to the morphological difference between the general human voxel model used in the simulation and the knee of our volunteer. Moreover, we believe that the slight discrepancies between the simulation and the experimental results could be also justified with a slight variation in sample positioning and alignment during workbench experiments with respect to the simulations: similar variations

are more relevant for superficial channel respect to the solenoid channel since the last one has a more homogeneous sensitivity.

Table 1 shows that for the solenoid channel the sample induced resistance is over 2-4 times greater than the coil resistance, being this coil characterized by a volumetric geometry with a good filling factor. The sample induced resistance of the superficial coil has got values which are comparable with the coil resistance ones, pointing out a condition of balance between sample-coil dominance.

Respect to the described application, at lower field strength the SNR is mainly determined by the coil losses while at higher field strength the sample losses are dominant (30). However, we believe that the knowledge of a sample-coil interaction model is very useful for the design of a system strictly coupled to the sample.

B_1 field distributions obtained from the simulation are congruent with the theory for both channels for all conditions. Comparing magnetic field homogeneity obtained for the solenoid channel by means of the simulation and the one directly obtained from real images (27), it is possible to conclude that the numerical estimation of this parameter is very accurate. Also, the B_1 field plots as a function of the y-axis for the coil loaded with homogeneous cylindrical phantom obtained from the simulations are very similar to those obtained from the real images, to confirm the accuracy of the numerical method.

All our simulations were performed using a personal computer (@ 2.67 GHz, RAM 4 GB) and had an average duration of about 5 hours.

These results confirm the possibility of using the FDTD method for research and development of MRI systems as a tool to evaluate and optimize complex RF coil design. The coil designer could effectively get quick feedback on the performance of the coil, without the time or cost of producing numerous prototypes. Since the process of MR image acquisition is sensitive to the electric and magnetic field spatial patterns of the RF coil in use, knowledge of the field propagation and distribution of these fields in the patient is very important for good quality images.

Prior published works on coil design using FDTD methods are mainly focused on birdcage (11, 14) or phase array coils (13) for the estimation of resonant modes and/or B1 field homogeneity at medium-high field ($\geq$1.5T). To our knowledge, this work is the first to analyze the performances in terms of Rsample and sensitivity of a two-channel coil with complex geometry, at low field. Despite this work focuses on a commercially available coil, we think that the methodology introduced can be followed also for the construction of a novel coil effectively before manufacturing. Then, once the most suitable design for the intended

application has been chosen, the designer can efficiently proceed with prototyping and workbench testing, saving significant resources as well as time to market.

The possibility to simulate the coil in practical use, under different loaded conditions, permits the designer to optimize the performance of the device ensuring a good product before any prototype are built. In this regard, possible future developments will concern the simulation of the knee coil in various loaded conditions, such as different positions of the sample with respect to the superficial channel, to analyze and optimize coil performance. Moreover, some geometrical changes may be made to the two coil channels in order to obtain an optimized configuration which will provide high quality images.

REFERENCES

1. S. Simi, M. Ballardin, M. Casella, D. De Marchi, V. Hartwig, G. Giovannetti, N. Vanello, S. Gabbriellini, L. Landini, M. Mut Res **645**, 39–43 (2008)
2. V. Hartwig, G. Giovannetti, N. Vanello, M. Lombardi, L. Landini, S. Simi. Int. J. Environ. Res. Public Health **6**, 1778-1798 (2009)
3. V. Hartwig, G. Giovannetti, N. Vanello, L. Landini, M.F. Santarelli. Appl. Magn. Reson. **38**, 337-348 (2010)
4. V. Hartwig, N. Vanello, G. Giovannetti, M. Lombardi, L. Landini, M.F. Santarelli. Magn. Reson. Mater. Phy. **24**, 323–330 (2011)
5. B.K. Rutt, D.H. Lee. JMRI **6**, 57-62 (1996)
6. A.D. Vellet, D.H. Lee, P.L. Munk, L. Hewett, M. Eliasziw, S. Dunlavy, L. Vidito, P.J. Fowler, A. Miniaci, A. Radiology **197,** 826-830 (1995)
7. P.M. Parizel, H.A. Dijkstra, G.P. Geenen, P.A. Kint, R.J. Versteylen, P.J. van Wiechen, A.M. De Schepper. Eur. J. Radiol. **19**, 132-138 (1995)
8. G. Giovannetti, V. Hartwig, L. Landini, M.F. Santarelli. Appl. Magn. Reson. **39,** 391–399 (2010)
9. G. Giovannetti, F. Frijia, V. Hartwig, V. Viti, L. Landini. Appl. Magn. Reson. **39(3)**, 225-231 (2010)
10. K.S. Yee. IEEE Trans. Ant. Propag. **14,** 302-307 (1966)
11. T.S. Ibrahim, R. Lee, B.A. Baertlein, Y. Yu, P.M.L. Robitaille. Magn. Reson. Imaging. **18**, 835-843 (2000)
12. C.M. Collins, M.B. Smith. Magn. Reson. Med. **45**, 692-699 (2001)
13. J.H. Seo, H.Y. Heo, B.H. Han, S.Y. Lee. In: Proceedings of the 29th Annual International Conference of the IEEE EMBS, Lyon, France, 2007, FrD03.6.

14. W. Liu, C.M. Collins, M.B. Smith. Appl. Magn. Reson. **29**, 5-18 (2005)
15. C. Guclu, G. Kashmar, A. Hacinliyan, O. Nalcioglu. Magn. Reson. Med. **37(1)**, 76–83 (1997)
16. J.H. Chen, S.K. Jeng, F.H. Lin, W.P. Kuan. IEEE Trans. Magn. **35(4),** 2118–2127 (1999)
17. G. Giovannetti, V. Viti, V. Hartwig, Y. Liu, W. Yu, R. Mittra, L. Landini, A. Benassi. Int. J. Biomedical Engineering and Technology **4(1),** 18-28 (2010)
18. G. Giovannetti, V. Hartwig, L. Landini, M.F. Santarelli. Appl. Magn. Reson. **40,** 351-361 (2011)
19. G. Giovannetti, V. Viti, L. Yongjun, W. Yu, R. Mittra, L. Landini, A. Benassi Concept Magn. Reson. B **33B(4)**, 209-215 (2008)
20. L. Darrasse, G. Kassab. Rev Sci Instrum **64 (7),** 1841-1844 (1993)
21. R. Hernandez, A. Rodriguez, P. Salgado, F.A. Rev. Mex. Fis. **49(2)**, 107-114 (2003)
22. Y. Duan, T.S. Ibrahim, B.S. Peterson, F. Liu, A. Kangarlu. Int. J. Antennas Propag. **1**,1-10 (2008)
23. American Society for Testing and Material (ASTM) Designation: F2182-02a (2004) Standard Test Method for Measurement of Radio Frequency Induced Heating Near Passive Implants During Magnetic Resonance Imaging, ASTM International, West Conshohocken, PA.
24. G. Giovannetti, V. Hartwig, V. Viti, P. Zadaricchio, L. Meini, L. Landini, A. Benassi. Concepts Magn. Reson. **33B(1),** 32–38 (2008)
25. D.I. Hoult. Concepts Magn. Reson. **12**,173–187 (2000)
26. C. Penney. Microwave J. **50(12)**, 118-122 (2007)
27. G. Giovannetti, V. Viti, V. Positano, M.F. Santarelli, L. Landini, A. Benassi. Int. J. Biomedical Engineering and Technology **1(1)**, 4-17 (2007)
28. J. Wang, A. Reykowski, J. Dickas. IEEE Trans. Biomed. Eng. **42(9)**, 908-917 (1995)
29. J.M. Jin, Electromagnetic Analysis and Design in Magnetic Resonance Imaging (CRC Press, Boca Raton, 1999)
30. G. Giovannetti, R. Francesconi, L. Landini, M.F. Santarelli, V. Positano, V. Viti, A. Benassi. Concept Magn. Reson. B **20B(1),** 9–16 (2004)

List of Figure captions

FIG. 1. Knee coil: CAD model (**a**) and picture (**b**)

FIG. 2. Matching network. Solenoid channel: C1=680 pF, C2=27 pF, L1=L2=0.675 μH; superficial channel: C1=820 pF, C2=27 pF, L1=L2=0.675 μH

FIG. 3. Knee coil in loaded conditions: homogenous cylindrical phantom (**a**), human model (**b**)

FIG. 4. B_1 field magnitude distributions for the knee coil loaded with human model (from left to right: axial, sagittal and coronal plane: solenoid channel (**a**), superficial channel (**b**). The dB values are relative to the B_1 in the center of the coil.

FIG. 5. Plot of the B_1 field as a function of the y-axis for the knee coil in different loaded conditions. Unloaded, loaded with homogeneous cylindrical phantom and loaded with human model: solenoid channel (**a**), superficial channel (**b**). Loaded with homogeneous cylindrical phantom simulation vs image results: solenoid channel (**c**), superficial channel (**d**). Red points in the graphs indicate the phantom extension.

TABLE 1. Workbench test and simulation results

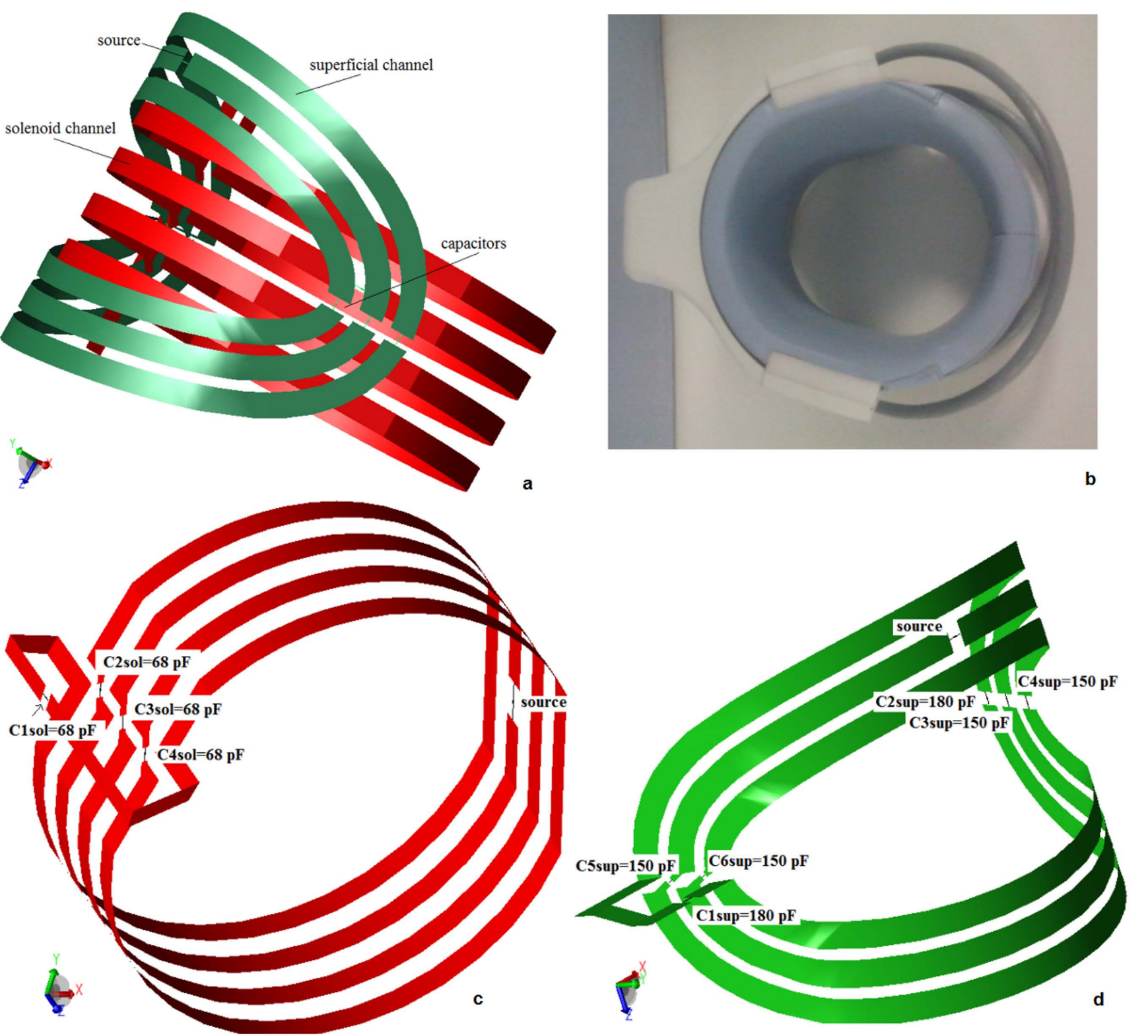

FIG. 1: Knee coil model: a) CAD model, b) picture, c) solenoid channel, d) superficial channel

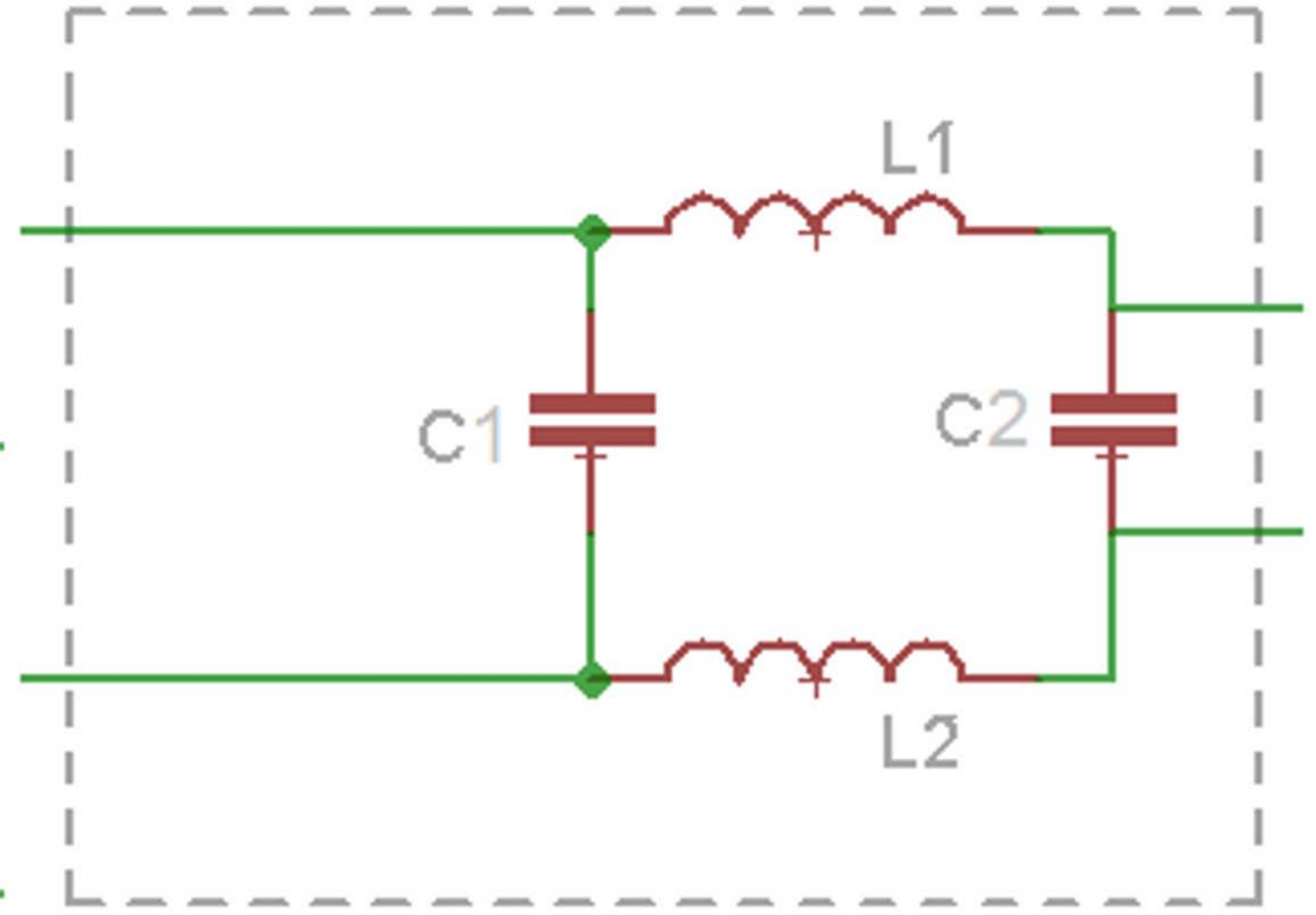

FIG. 2. Matching network. Solenoid channel: C1=680 pF, C2=27 pF, L1=L2=0.675 uH; superficial channel: C1=820 pF, C2=27 pF, L1 =L2=0.675 uH

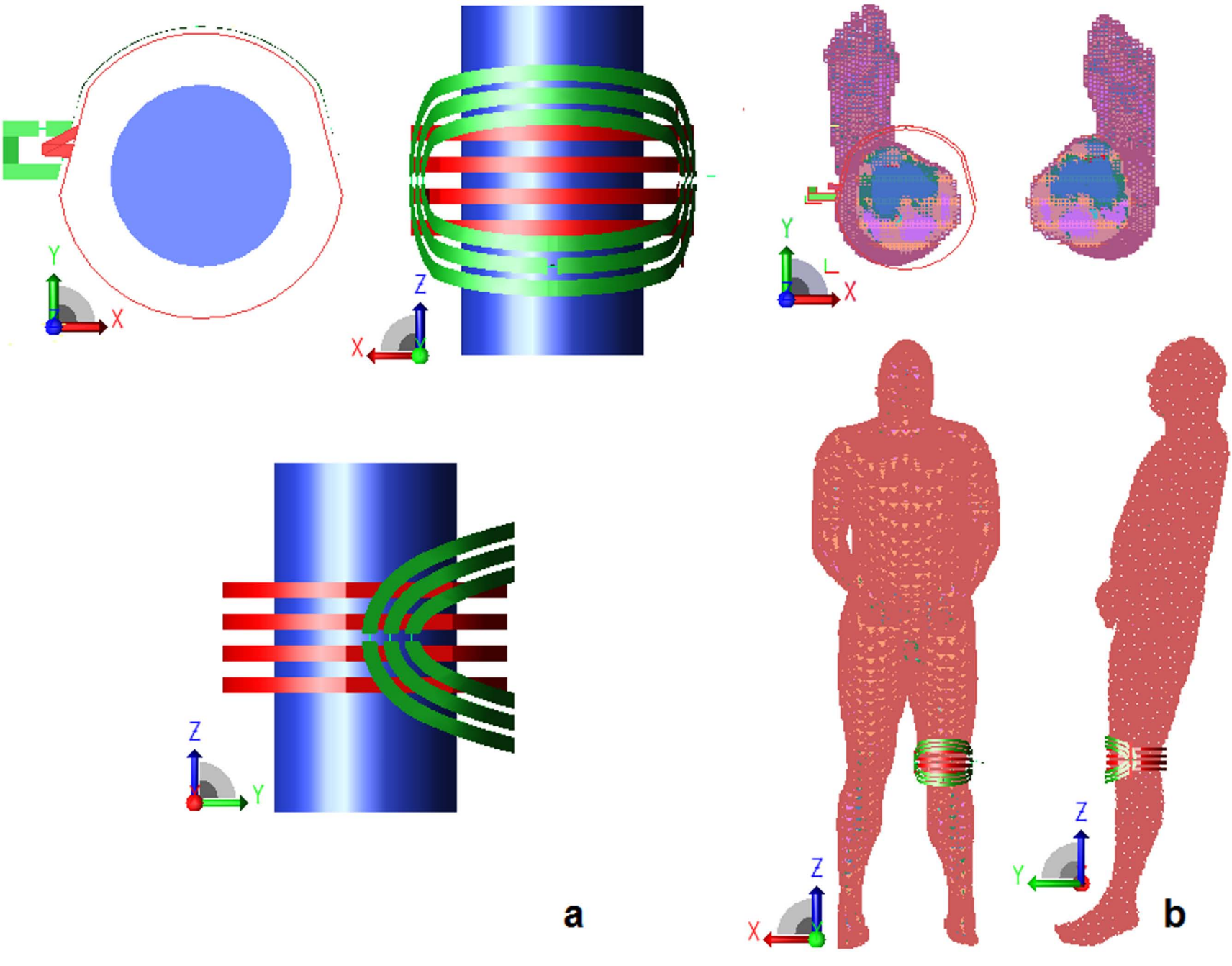

FIG. 3. Knee coil in loaded conditions: homogeneous cylindrical phantom (**a**), human model (**b**)

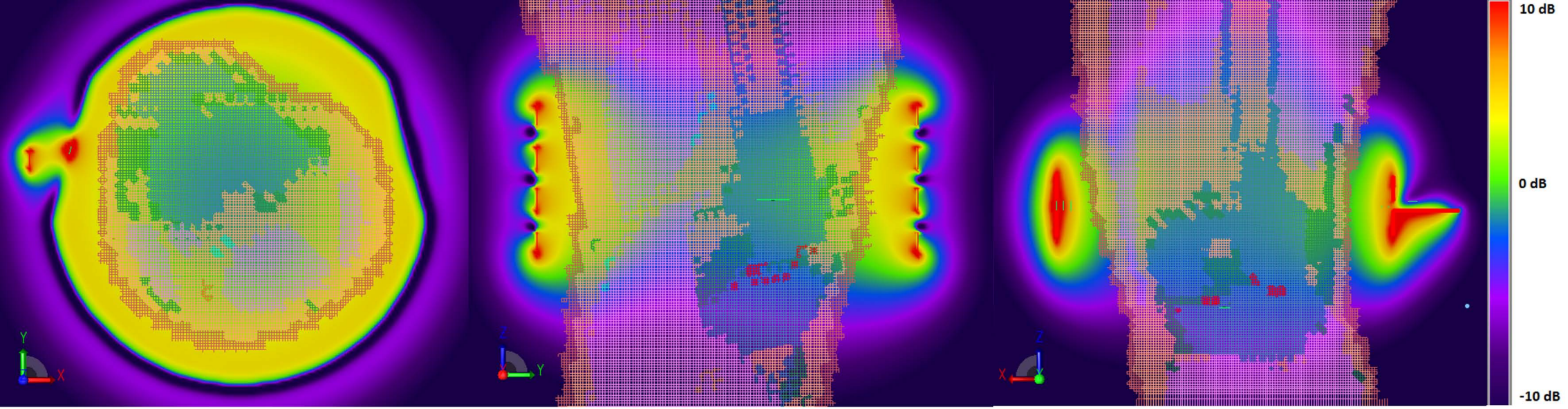

a)

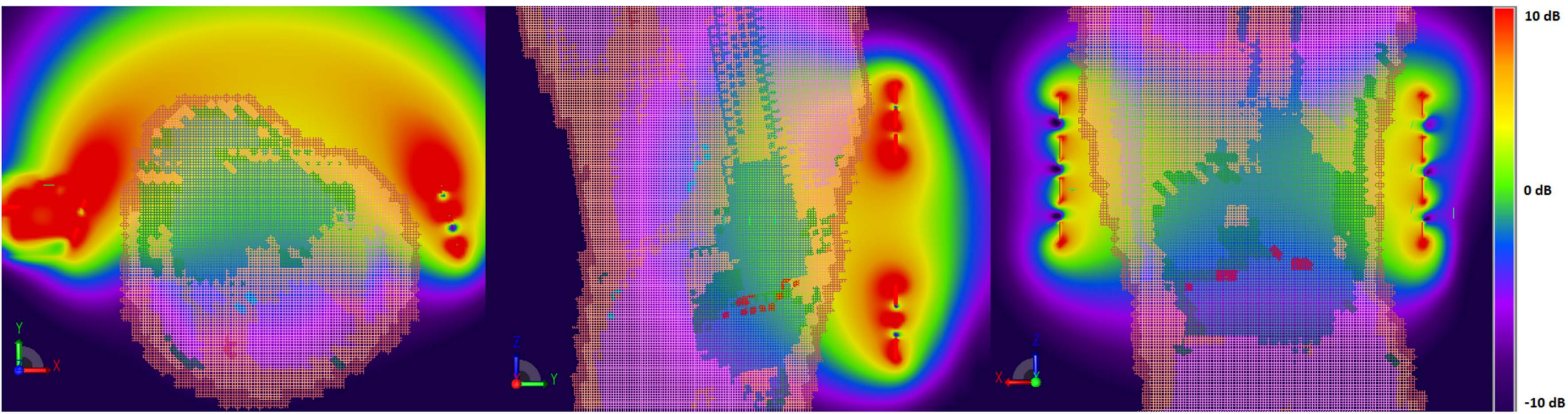

b)

FIG. 4. B1 field magnitude distributions for the knee coil loaded with human model (from left to right: axial, sagittal and coronal plane): solenoid channel (a), superficial channel (b). The dB values are relative to the B1 in the center of the coil.

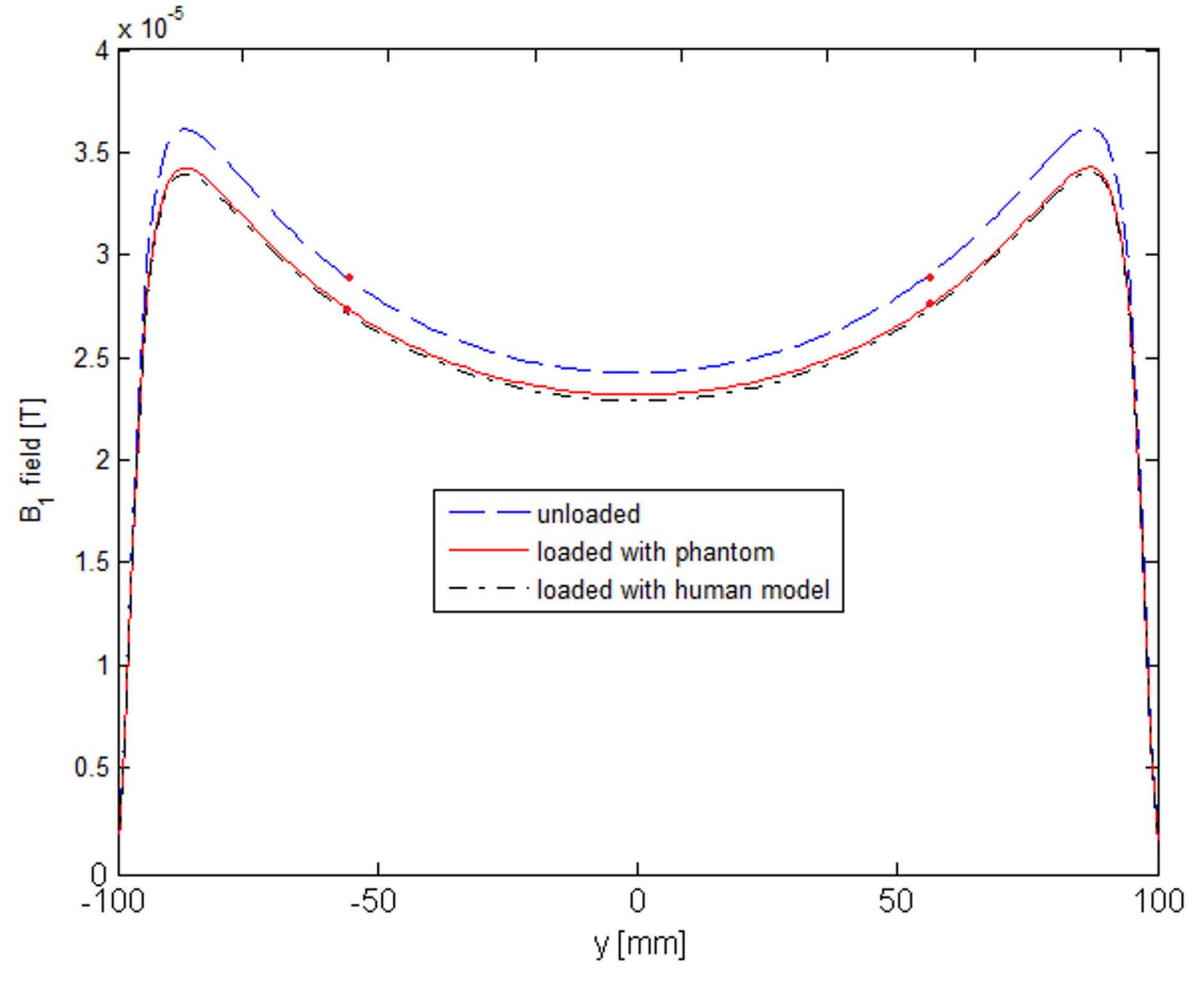

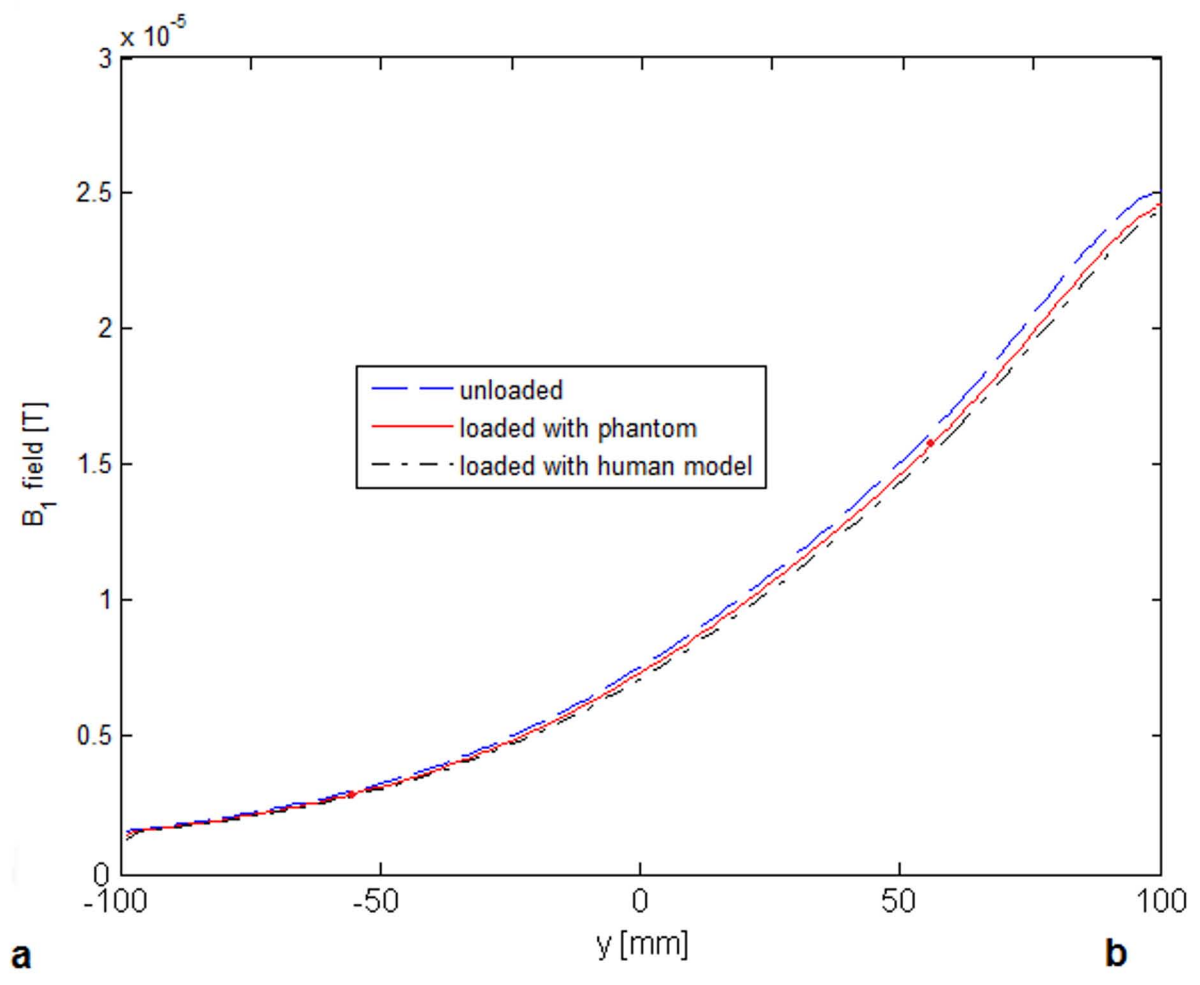

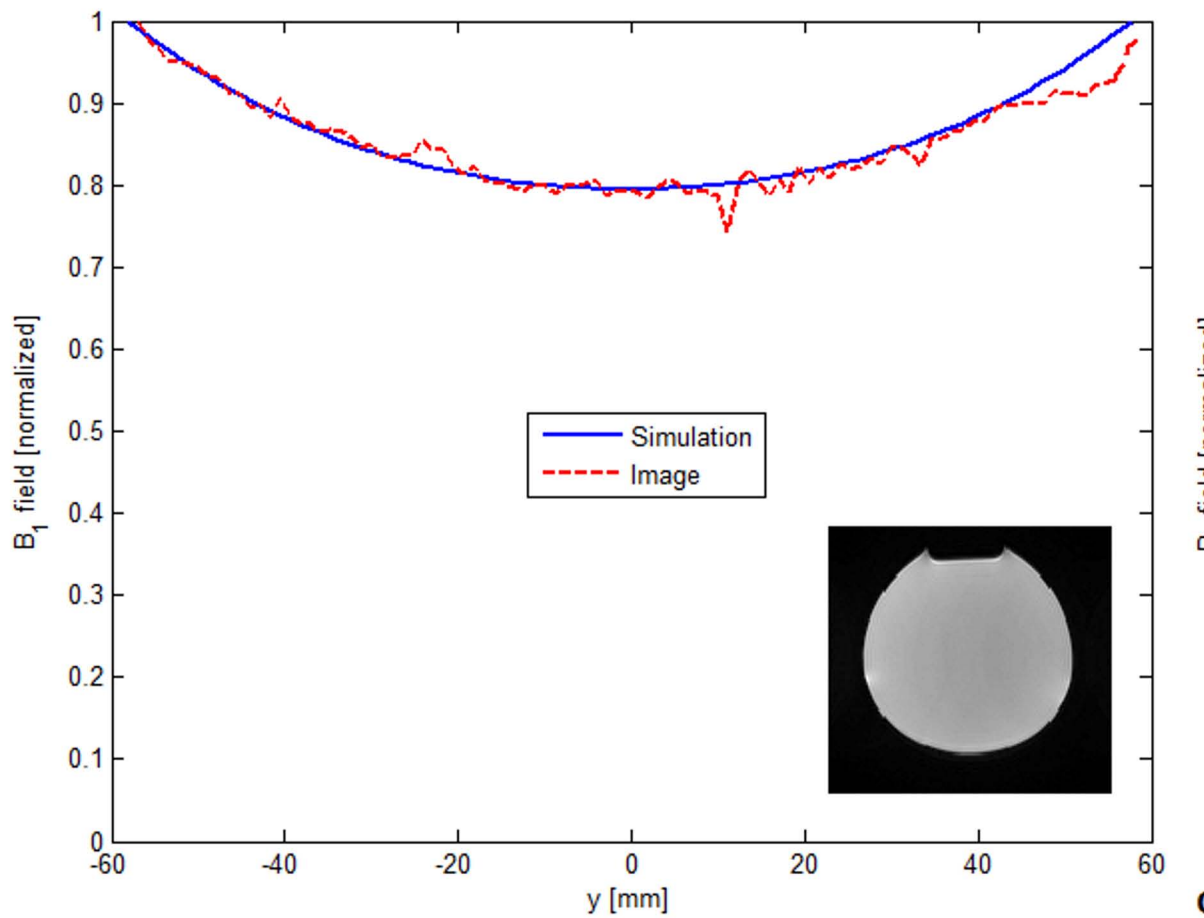

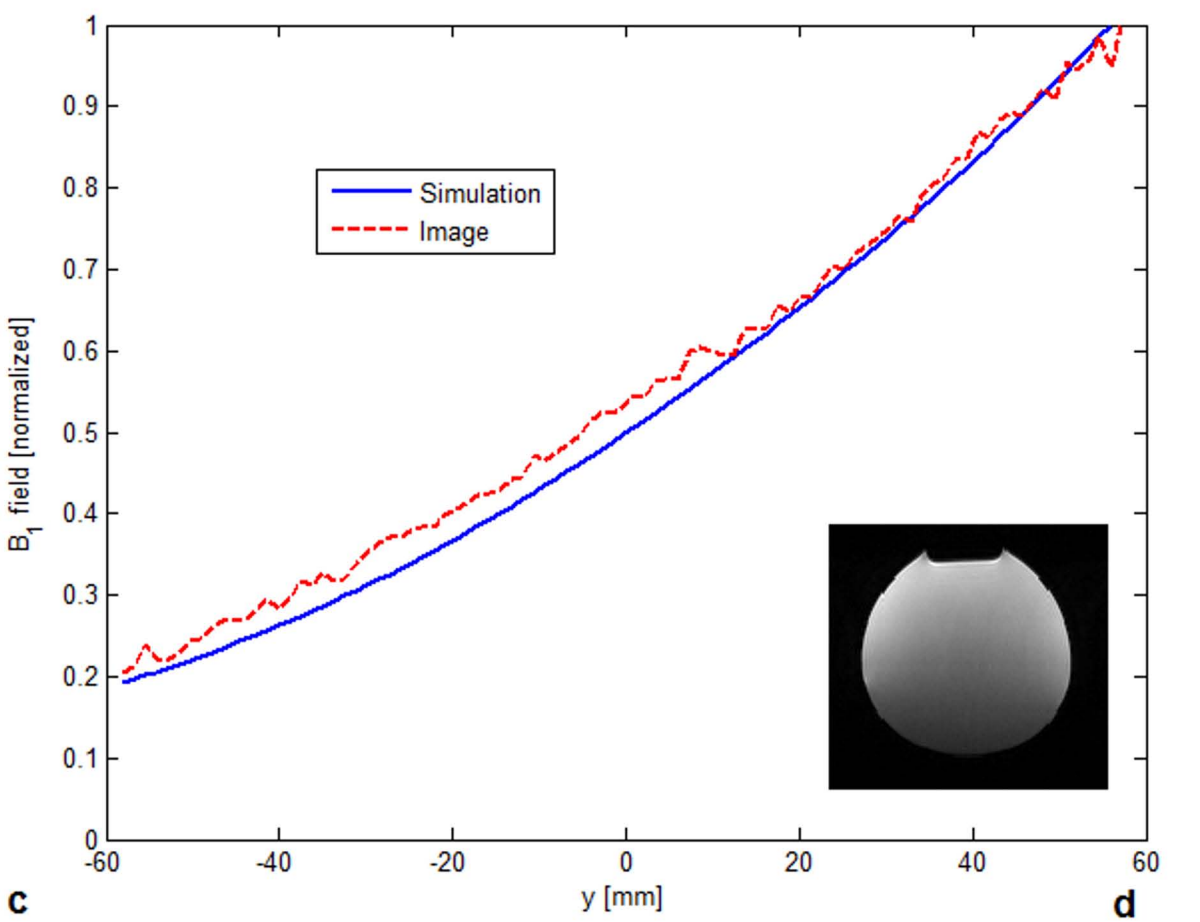

FIG. 5 . Plot of the B1 field as a function of the y-axis for the knee coil in different loaded conditions. Unloaded, loaded with homogeneous cylindrical phanto and loaded with human model: solenoid channel (a), superficial channel (b). Loaded with homogeneous cylindrical phantom simulation vs image results: solenoid channel (c), superficial channel (d). Red points in the graphs indicate the phantom extension.

Table 1. Workbench test and simulation results

	f_0 (MHz)	B (kHz)	Q	Rsample (Ω)	Rcoil (Ω)	R_s XFdtd (Ω)	Error (@ f_0 = 21.3 MHz)
Unloaded SOL	21.36	55.64	384	-	1.31	-	-
SOL + cylindrical phantom	21.36	208.20	103	3.61	1.31	3.39 (@ f_0 = 20.5141 MHz)	1.1 %
SOL + human knee	21.35	300.00	78	5.14	1.31	4.79 (@ f_0 = 20.7771MHz)	2.1 %
Unloaded SUP	21.48	65.80	326	-	1.01	-	-
SUP + cylindrical phantom	21.47	143.7	149	1.19	1.01	1.03 (@ f_0 = 20.2832 MHz)	4.6 %
SUP + human knee	21.46	170.7	126	1.6	1.01	1.26 (@ f_0 = 20.2758 MHz)	12.5 %